Journal of Applied Mechanics and Technical Physics, Vol. 43, No. 4, pp. 503–511, 2002

OSCILLATIONS OF CYLINDERS IN A LINEARLY STRATIFIED FLUID

E. V. Ermanyuk and N. V. Gavrilov

UDC 532.59

The paper studies theoretically and experimentally hydrodynamic loads that act on horizontally placed cylinders of rhombic and square cross sections, oscillating harmonically in a linearly stratified fluid. An analytical solution is found with the use of affine similitude. Hydrodynamic force coefficients were evaluated experimentally from Fourier transforms of records of damped oscillations in a time–frequency region. It is shown that for polygonal contours, hydrodynamic loads change abruptly if the slope of the polygon sides coincides with the slope of the internal-wave group velocity vector.

Introduction. Local characteristics of the field of internal waves generated by harmonic oscillations of bodies immersed in an exponentially stratified fluid have been studied theoretically and experimentally [1–4]. Several papers assess integral characteristics, such as the power expended for internal wave radiation and the hydrodynamic load acting on oscillating bodies. Gorodtsov and Teodorovich [5] proposed an approximate method for estimating the radiation power, in which a body is simulated by a distribution of special features obtained as a solution of the problem for a heterogeneous fluid.

Estimates of hydrodynamic loads for vertical oscillations of an ellipsoid of revolution [6] and arbitrary oscillations of an elliptic cylinder [7] were obtained in the Boussinesq approximation for an inviscid exponentially stratified fluid with strict satisfaction of the nonpenetration condition on the body. Hurley and Keady [8] extended the solution of [7] to a viscous fluid. Ermanyuk [9] tested experimentally Keady's solution. We note that the solutions of [6, 7] were constructed for particular body geometries and the method used in these studies cannot be applied to bodies of arbitrary geometries. A solution for such bodies can be obtained using the relations of affine similitude [10]. Ermanyuk [10] also gave experimental data for ellipses of revolution of various lengths.

In the present paper, the relations obtained in [10] are used to estimate theoretically the hydrodynamic loads acting on horizontal cylinders of rhombic and square cross sections oscillating horizontally and vertically in an exponentially stratified fluid. The solutions for horizontal oscillations were verified experimentally by using the technique described in [9]. We note that the motion of contours with angular points in a stratified fluid was studied only by Dalziel [11], who investigated experimentally the structure of the field of internal waves generated by vertical oscillations of a square contour. The problem of contours with angular points oscillating in a viscous inhomogeneous fluid is studied in detail in [12].

1. Theoretical Analysis. In the present paper, the problem of oscillations of flat contours in an exponentially stratified fluid is a particular case of the problem of oscillations of three-dimensional bodies [10]. Governing relations for the spatial case are formulated, and special features of the flat problem are studied. As in [10], we use the model of an unbounded inviscid incompressible stratified fluid with the constant Brunt–Väisälä frequency $N(x_3) = \sqrt{-(g/\rho)(d\rho/dx_3)} = \text{const}$ [$\rho(x_3)$ is the density distribution over the vertical in the Cartesian coordinates (x_1, x_2, x_3) and g is the acceleration of gravity].

The following physical considerations determine the range of parameters in which this model can be used. Generally, a hydrodynamic load on a body of characteristic dimension L which is oscillating harmonically with amplitude a and frequency ω in a viscous stratified fluid with $N = \text{const}$ depends on the three main parameters:

Lavrent'ev Institute of Hydrodynamics, Siberian Division, Russian Academy of Sciences, Novosibirsk 630090.
Translated from Prikladnaya Mekhanika i Tekhnicheskaya Fizika, Vol. 43, No. 4, pp. 15–26, July–August, 2002. Original article submitted August 17, 2001; revision submitted March 11, 2002.

0021-8944/02/4304-0503 $27.00

the dimensionless oscillation frequency $\Omega = \omega/N$, the Keulegan–Carpenter number a/L, and the Stokes number $\beta = L^2\omega/\nu$ (ν is the kinematic viscosity of the fluid). For an ideal fluid with $N = \text{const}$, the main parameter is the dimensionless frequency Ω, which acts as the Froude number in the present problem.

The scale of hydrodynamic loads in an ideal fluid depends on the body volume W. In a viscous fluid with $\beta \gg 1$ and $a/L \ll 1$, an oscillating body is surrounded by a boundary layer of thickness of order $\delta^* = \sqrt{\nu/\omega}$. Correspondingly, the fluid volume in which intense viscous dissipation of energy occurs in the vicinity of the body is of order $\delta^* S$ (S is the surface area of the body). The viscous and inviscid effects are approximately characterized by the quantity $A = \delta^* S/W$. For large A, the viscous effect becomes dominant. For example, if a thin plate (body of zero volume) oscillates in its plane, $A \to \infty$ and the viscous effect should be taken into account [13, 14].

If $a/L \approx 1$, flow separation occurs in the vicinity of the body, which implies an increase in the effective thickness β and parameter A. For bodies with angular points, separation occurs for relatively small a/L. The theory of [12], which holds for $a/L < 0.5$, allows estimation of the hydrodynamic loads on cylinders with rhombic and square cross sections in a heterogeneous fluid. For the range of parameters studied in the present paper, the estimated effect of flow separation on oscillation characteristics is negligibly small because for $a/L \ll 1$ and $\beta \gg 1$, viscous effects in a thin boundary layer around the body make a major contribution (linear in a/L) to damping, whereas the contribution of local flow separations at the angular points is of order of $(a/L)^2$. Obviously, this estimate is also valid for a stratified fluid because in a small locality of the angular points, the local flow velocity is high, and, hence, the contribution of local inertial effects determining flow separation is greater than that of the buoyancy effects.

We note that in some cases of large a/L, in the vicinity of a body oscillating in a stratified fluid, structures affecting the oscillation dynamics are formed (see, for example, a description of vortex and spear-shaped structures in [15]). In the present paper, we do not consider this complex nonlinear problem.

The above considerations suggest that the model of an ideal stratified fluid used here gives adequate estimates of real hydrodynamic loads for $a/L \ll 1$, $A \ll 1$, and $\beta \gg 1$.

Below, the equations of fluid motion are written for the "internal" potential [16]. If we assume that the body motion velocity $\boldsymbol{v}^{(1)}$, the "internal" potential $\varphi^{(1)}$, the fluid particle velocity $\boldsymbol{u}^{(1)}$, and the pressure $p^{(1)}$ are harmonic functions of time in the form $\boldsymbol{v}^{(1)}(x_1, x_2, x_3, t) = \boldsymbol{V}^{(1)}(x_1, x_2, x_3)\mathrm{e}^{i\omega t}$, the following problem can be formulated.

Problem 1. The equation of fluid motion has the form

$$\Big(\frac{\partial^2}{\partial x_1^2} + \frac{\partial^2}{\partial x_2^2} + \frac{1}{\alpha^2}\,\frac{\partial^2}{\partial x_3^2}\Big)\Phi^{(1)} = 0, \tag{1}$$

where $\alpha = (\Omega^2 - 1)^{1/2}/\Omega$. Equation (1) can be either an elliptic or hyperbolic equation, depending on the sign of α^2. First, we consider the elliptic problem ($\alpha^2 > 0$). The pressure and velocity of the fluid particles in Problem 1 are expressed in terms of the potential as follows:

$$P^{(1)} = -\rho_0 i\omega\Phi^{(1)}, \qquad \boldsymbol{U}^{(1)} = \Big(\frac{\partial}{\partial x_1}, \frac{\partial}{\partial x_2}, \frac{1}{\alpha^2}\,\frac{\partial}{\partial x_3}\Big)\Phi^{(1)}.$$

Here ρ_0 is the characteristic density. The boundary condition on the body surface $S^{(1)}$ specified by the equation $F^{(1)}(x_1, x_2, x_3) = 0$ has the form

$$\boldsymbol{U}^{(1)} \cdot \nabla^{(1)} F^{(1)} = \boldsymbol{V}^{(1)} \cdot \nabla^{(1)} F^{(1)}, \tag{2}$$

where $\nabla^{(1)} = (\partial/\partial x_1, \partial/\partial x_2, \partial/\partial x_3)$. At infinity, we impose the condition $\Phi^{(1)} \to 0$ as $x_1^2 + x_2^2 + x_3^2 \to \infty$.

After affine transformation of the coordinate system

$$\xi_j = a_j x_j, \qquad a_j = (1, 1, \alpha), \tag{3}$$

Problem 1 is converted to following problem.

Problem 2. The equation of fluid motion (1) is transformed into the Laplace equation

$$\Big(\frac{\partial^2}{\partial \xi_1^2} + \frac{\partial^2}{\partial \xi_2^2} + \frac{\partial^2}{\partial \xi_3^2}\Big)\Phi^{(2)} = 0. \tag{4}$$

The boundary condition on the surface $S^{(2)}$ specified by the function $F^{(2)}(\xi_1, \xi_2, \xi_3) = 0$ takes the form

$$\nabla^{(2)}\Phi^{(2)} \cdot \nabla^{(2)} F^{(2)} = \boldsymbol{V}^{(2)} \cdot \nabla^{(2)} F^{(2)}, \tag{5}$$

where $\nabla^{(2)} = (\partial/\partial\xi_1, \partial/\partial\xi_2, \partial/\partial\xi_3)$. The body velocity components are expressed similarly to (3): $V_j^{(2)} = a_j V_j^{(1)}$. At infinity, we specify the condition $\Phi^{(2)} \to 0$ as $\xi_1^2 + \xi_2^2 + \xi_3^2 \to \infty$.

The components of the hydrodynamic load vector $\boldsymbol{y}^{(1,2)}(t) = \boldsymbol{Y}^{(1,2)}\mathrm{e}^{i\omega t}$ in Problems 1 and 2 are determined by integration of the pressure $P^{(1,2)} = -\rho_0 i\omega\Phi^{(1,2)}$ over the body surface:

$$Y_k^{(1,2)} = -\rho_0 i\omega \int\limits_{S^{(1,2)}} \Phi^{(1,2)} n_k^{(1,2)}\, dS^{(1,2)}.$$

Here $n_k^{(1,2)}$ are the components of the unit vector of the internal normal to the body surface $S^{(1,2)}$.

It follows from Eqs. (4) and (5) that Problem 2 is a classical problem of oscillations of a body in an ideal heterogeneous fluid. It is known that in Problem 2, the hydrodynamic load components can be expressed in terms of the added-mass tensor components (see, for example, [17]):

$$y_k^{(2)} = -\sum_{j=1}^{3} m_{jk}^{(2)} \frac{dv_j^{(2)}}{dt}. \tag{6}$$

Here $v_j^{(2)} = V_j^{(2)}\,\mathrm{e}^{i\omega t}$ are the body velocity components. The components of the added mass tensor

$$m_{jk}^{(2)} = \rho_0 \int\limits_{S^{(2)}} \Phi_j^{(2)} n_k^{(2)}\, dS^{(2)} \tag{7}$$

are determined from the solution of Problem 2 for unit potentials, which are described by the expansion

$$\Phi^{(2)} = \sum_{j=1}^{3} V_j^{(2)} \Phi_j^{(2)}. \tag{8}$$

For Problem 1 [Eqs. (1) and (2)], relations similar to (6)–(8) can be introduced. In [10], for the added mass coefficient tensors $K_{jk}^{(1)} = m_{jk}^{(1)}/(\rho_0 W^{(1)})$ and $K_{jk}^{(2)} = m_{jk}^{(2)}/(\rho_0 W^{(2)})$ [$W^{(1)}$ and $W^{(2)}$ are the volumes of bodies surrounded by the surfaces $S^{(1)}$ and $S^{(2)}$], the following relation was obtained:

$$K_{jk}^{(1)} = K_{jk}^{(2)} a_j a_k. \tag{9}$$

For bodies of definite geometrical shapes with various ratios $e = b_2/b_1$ and $q = b_3/b_2$ of characteristic ellipse dimensions b_1, b_2, and b_3 in the directions ξ_1, ξ_2, and ξ_3, the components of the added mass coefficient tensors in Problem 2 are written in the form [18]

$$K_{jk}^{(2)} = f_{jk}(e, q). \tag{10}$$

For specified e_0 and q_0, the solution of Problem 1 for the added mass coefficient tensor can be obtained from Eqs. (9) and (10):

$$K_{jk}^{(1)}(\Omega) = f_{jk}(e_0, q_0\alpha) a_j a_k. \tag{11}$$

We note that in [19], relations of the type of (9) were obtained for the elliptic problem of a body moving under the law $\boldsymbol{v}(t) = \varepsilon \boldsymbol{v}_0 \mathrm{e}^{\delta t}$, where $|\boldsymbol{v}_0| = 1$ and ε and δ are small positive quantities. Vladimirov and Il'in [19] determined the asymptotic behavior for small velocities.

If $\Omega < 1$, Eq. (1) is a hyperbolic equation ($\alpha^2 < 0$). A special feature of the hyperbolic problem is the radiation of internal waves by the oscillating body. In this case, the problem can be solved using the analytic continuation

$$K_{jk}^{(1)}(\Omega) = f_{jk}(e_0, -q_0 i\eta)\gamma_j\gamma_k, \tag{12}$$

where $\eta = (1 - \Omega^2)^{1/2}/\Omega$ and γ_j and γ_k are 1, 1, and $-i\eta$ for j, $k = 1$, 2, and 3, respectively. We note that unlike in the case of $\Omega > 1$ where $m_{jk}^{(1)}$ are real quantities, for $\Omega < 1$, the quantities $m_{jk}^{(1)}$ are generally complex. In marine hydrodynamics, the representation $m_{jk} = \mu_{jk} - i\lambda_{jk}/\omega$ [17] is commonly accepted, where μ_{jk} is the added mass and λ_{jk} is the damping coefficient. The corresponding dimensionless quantities have the form

$$C_{jk}^{\mu} = \mu_{jk}/(\rho_0 W^{(1)}) = \mathrm{Re}\,(K_{jk}^{(1)}), \qquad C_{jk}^{\lambda} = \lambda_{jk}/(\rho_0 N W^{(1)}) = \Omega\,\mathrm{Im}\,(K_{jk}^{(1)}). \tag{13}$$

Equations (11) and (12) suggest that in the case of bodies with different q_0 and fixed e_0, the following relations of affine similitude are valid:

$$K_{jk}^{(1)}/(a_j a_k) = \mathrm{idem} \quad \text{if} \quad q_0^2\alpha^2 = \mathrm{idem}. \tag{14}$$

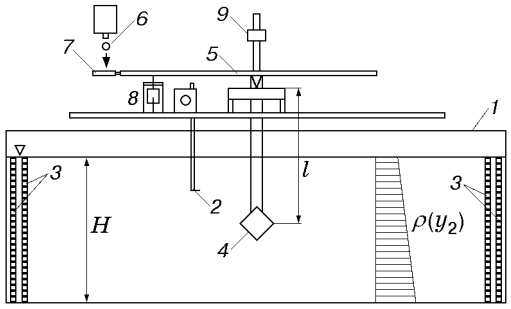

Fig. 1. Diagram of the experimental installation: 1) test tank; 2) conductivity probe; 3) wave breakers; 4) cylinder with square cross section; 5) pendulum; 6) steel ball; 7) rubber membrane; 8) electrolytic displacement sensor; 9) counterbalance.

For the spatial problem of horizontal oscillations of a body as $\Omega \to 0$ ($\alpha^2 \to -\infty$), Eq. (1) with boundary condition (2) is reduced to a set of two-dimensional Laplace equations with the corresponding nonpenetration conditions on horizontal cross sections of the body. The value of C^{μ}_{11} as $\Omega \to 0$ can be calculated by the flat cross section method. As $\Omega \to 0$, the imaginary part of hydrodynamic load coefficients vanishes.

In the two-dimensional problem, instead of the coordinates (x_1, x_2, x_3), we use the coordinates (y_1, y_2) in the plane $x_1 = 0$ so that $y_1 = x_2$ and $y_2 = x_3$. In this case, the transformations of formulas (10)–(13) are obvious. The quantities C^{μ}_{mn} and C^{λ}_{mn} (m and n take values of 1 and 2) are load coefficients per unit of length, and the quantities $W^{(1)}$ and $W^{(2)}$ are the cross-sectional areas of horizontal cylinders in Problems 1 and 2. In addition, in the flat problem, the functions f_{mn} included in relations (10)–(12) are functions of the same parameter q. The limiting transition $\Omega \to 0$ corresponds to $|q| \to \infty$. However, as $|q| \to \infty$, any flat contour degenerates into a vertical line. Hence, for horizontal oscillations as $\Omega \to 0$, only the vertical dimension of the cylinder matters but not the shape of its cross section. For a cylinder of cross-sectional area $W^{(1)}$ and vertical dimension D, we can find the limiting value of $C^{\lambda}_{11}(\Omega)$ as $\Omega \to 0$: $C^{\lambda}_{11}(0) = \pi D^2/(4W^{(1)})$. For example, $C^{\lambda}_{11}(0) = 1$ for a circle, $\pi/2$ for a rhombus with a vertical diagonal, and $\pi/4$ for a square.

For an ellipse, the functions $f_{mn}(q)$ have the simple form: $f_{11}(q) = q$ and $f_{22}(q) = 1/q$. For a cylinder of rhombic cross section with a vertical diagonal, the functions f_{mn} are given in [18]. In particular, for horizontal oscillations of such a cylinder, the following relation holds:

$$f_{11}(q) = \frac{\Gamma[3/2 - \arctan\,(1/q)/\pi]\Gamma[\arctan\,(1/q)/\pi]}{\Gamma[1/2 - \arctan\,(1/q)/\pi]\Gamma[1 - \arctan\,(1/q)/\pi]} - 1. \tag{15}$$

Here Γ is the Eulerian gamma function. For horizontal oscillations of a rectangle, the function f_{11} is given by [18]

$$f_{11}(q) = \pi q(1 - k^2)(E(æ) - k^2 G(æ))^{-2}/4 - 1, \tag{16}$$

where $æ = (1 - k^2)^{1/2}$ and k is a root of the equation

$$E(æ) - k^2 G(æ) = q(E(k) - (1 - k^2)G(k)). \tag{17}$$

Here $G(k) = \int\limits_0^{\pi/2} (1 - k^2 \sin^2 \varphi)^{-1/2}\, d\varphi$ and $E(k) = \int\limits_0^{\pi/2} (1 - k^2 \sin^2 \varphi)^{1/2}\, d\varphi$ are total elliptic first- and second-type integrals. In the case of vertical oscillations of the rhombus and square, the functions f_{22} are obtained by substitution of the variable $1/q$ for q on the right sides of (15)–(17). A comparison of the theoretical relations derived from Eqs. (11) and (12) using Eqs. (15) and (16) is given in the experimental part of the present paper (Sec. 3).

2. Experimental Method. A diagram of the experimental installation is shown in Fig. 1. The experiments were performed in a $2 \times 0.4 \times 0.15$ m test tank filled with a linearly stratified fluid with layer thickness $H = 0.36$ m. The fluid (solution of sugar) was poured by layers 2 cm thick with specified density difference between the layers. The linear density distribution due to molecular diffusion was determined after 48 hours. The density distribution over thickness was measured by a conductivity probe calibrated on samples of the solution of specified densities.

The operation of the probe is based on the principle that the conductivity of sugar solved in distilled water increases with increase in sugar concentration, and, hence, solution density.

The experiments were conducted for buoyancy frequency $N = 1\ sec^{-1}$, fluid layer thickness $H = 0.36$ m, temperature $T = 15°C$, solution density near the tank bottom $\rho_{\max} = 1.035$ g/cm^3, and viscosity $\nu_{\max} = 1.64 \times 10^{-3}$ g/(cm $\cdot$ sec). The effect of the buoyancy frequency N on hydrostatic load coefficients was studied in [20]. The tank butt-ends were equipped with wave breakers. A cylinder with 3.7×3.7 cm square cross section was fixed at the low streamline end of a physical pendulum in two positions such that either its side or diagonal were oriented vertically. Pendulum motion was initiated by a steel ball falling on a rubber membrane. The pendulum response was recorded by an electrolytic displacement sensor and processed by a personal computer. The coefficient of the restoring moment of the pendulum was varied by changing the vertical coordinate of the counterbalance of mass $m = 188$ g. Techniques for signal processing and estimating the dependences of dynamic characteristics of oscillating bodies on frequency are given in [9].

The response of a linear system to the action of an arbitrary perturbation force $h(t)$ can be written as

$$\zeta(t) = \int_0^\infty r(\tau) h(t-\tau)\, d\tau,$$

where $r(t)$ is the system response to a unit pulse. In the particular case of a harmonic perturbation force $h(t)=h_0 e^{i\omega t}$, we have

$$\zeta(t) = f_0 R(\omega)\, e^{i\omega t}. \tag{18}$$

Here $R(\omega) = R_c(\omega) - iR_s(\omega) = \int_0^\infty r(\tau)\, e^{-i\omega\tau}\, d\tau$ is the system response to a unit perturbating action in the frequency range and $R_c(\omega)$ and $R_s(\omega)$ are the cosine and sinus Fourier transforms, respectively.

The equation of horizontal oscillations of the cylinder under the action of a harmonic perturbation force can be written as

$$[M + \mu_{11}(\omega)]\, \frac{d^2x_1}{dt^2} + \lambda_{11}(\omega)\, \frac{dx_1}{dt} + c_{11}x_1 = h_0\, e^{i\omega t}, \tag{19}$$

where $M = J/l^2$ is the mechanical inertia of the system, J is the moment of inertia of the pendulum with respect to the axis of rotation, l is the distance from the axis of pendulum rotation to the center of the body, and c_{11} is the coefficient of the restoring force determined by statistical calibration. We note that $J = J_0 + mz^2$ ($J_0 = 1.12 \times 10^6$ g $\cdot$ cm^2 is the intrinsic moment of inertia of the pendulum with respect to the axis of rotation and z is the elevation of the center of gravity of the counterbalance above the axis of rotation of the pendulum). Setting $x_1 = \zeta$ and substituting (18) into (19), we obtain the following dependences of the added mass and the damping coefficient on the frequency:

$$\mu_{11}(\omega) = \frac{c_{11}}{\omega^2}\Big(1 - \frac{|R(0)|}{|R(\omega)|}\cos\theta(\omega)\Big) - M, \qquad \lambda_{11}(\omega) = \frac{c_{11}}{\omega}\,\frac{|R(0)|}{|R(\omega)|}\sin\theta(\omega), \tag{20}$$

where $|R(\omega)| = (R_c^2(\omega) + R_s^2(\omega))^{1/2}$, $\theta(\omega) = \arcsin(R_s(\omega)/R_c(\omega))$, and $|R(0)|$ is the value of $|R(\omega)|$ as $\omega \to 0$. By normalizing $|R(\omega)|/|R(0)|$, we process experimental records of damped oscillations obtained for an arbitrary initial pulse.

Using the technique described, responses $r(t)$ were recorded by a 12-bit analog-to-digital converter at a sampling frequency of 20 Hz. Then, we calculated the function $R(\omega)$ using a standard fast Fourier transform and estimated $\mu_{11}(\omega)$ and $\lambda_{11}(\omega)$ by formulas (20). To obtain reliable information for the frequency range, we processed 6–10 records of $r(t)$ for various positions of the counterbalance corresponding to various values of c_{11}. The maximum horizontal deflection of the body center in the experiments was $r_{\max}/L < 0.05$ (L is the side length of the square cross section of the cylinder). Thus, the experimental results obviously correspond to harmonic oscillation amplitudes $a/L < 0.05$.

Obvious technical difficulties hindered obtaining information for $\Omega \to 0$ and $\Omega \to \infty$. In fact, we studied the range of $0.2 < \Omega < 2$. In this case, the Stokes parameter was varied within $230 < \beta < 2300$. The value of A did not exceed 0.2. Thus, the parameter range studied in our experiments matches the parameter range in which the theoretical model used is applicable (see Sec. 1).

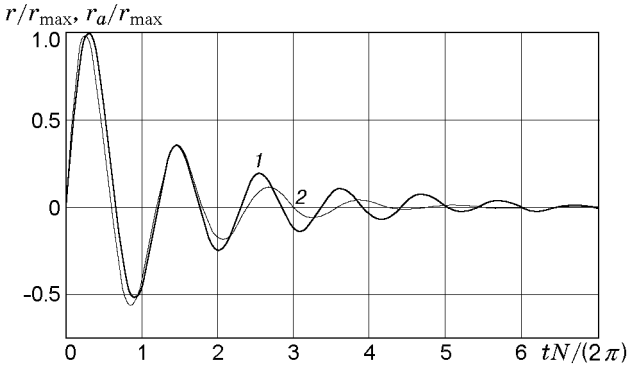

Fig. 2. Typical record of damped horizontal oscillations of the center of the rhombus $r(t)/r_{\max}$ (curve 1) and its approximation by the least-squares method $r_a(t)/r_{\max}$ (curve 2) for $z = 115$ mm and $\omega_* = 0.83$ sec^{-1}.

3. Theoretical and Experimental Results. Figure 2 shows a typical record of damped horizontal oscillations of the center of the rhombus $r(t)/r_{\max}$ in a continuously stratified fluid for $z = 115$ mm (curve 1). The time is normalized to the buoyancy period $2\pi/N$. The main qualitative features of the process follow from a comparison of $r(t)/r_{\max}$ with the approximation $r_a(t)/r_{\max} = B\,\mathrm{e}^{-kt}\sin(\omega_* t)$ obtained by the least-squares method. Using this method, we found the values of B, k, and ω_* minimizing the functional

$$I(B,k,\omega_*) = \int_0^\infty [r(t)/r_{\max} - B\,\mathrm{e}^{-kt}\sin(\omega_* t)]^2\,dt.$$

For a curve of $r_a(t)/r_{\max}$ (curve 2 in Fig. 2), $B = 0.96$, $k = 0.06$ sec^{-1}, and $\omega_* = 0.83$ sec^{-1}.

The curve of $r_a(t)/r_{\max}$ is a response of a linear oscillator whose inertial and damping characteristics do not depend on the oscillation frequency. Oscillations of this oscillator are described by an equation of the type of (19) whose coefficients are all constant. The oscillation period of the curve of $r_a(t)/r_{\max}$ specified by $2\pi/\omega_*$ is constant. It follows from Fig. 2 that the oscillation period of the curve of $r(t)/r_{\max}$ decreases with time. Theoretical studies of "memory" systems, whose oscillations are accompanied by wave radiation [21], show that as $t \to 0$ and $t \to \infty$, the inertial properties of such systems are determined by $\mu(\infty)$ and $\mu(0)$, respectively. The fact that the oscillation period decreases with time suggests the existence of the inequality $\mu(\infty) > \mu(0)$ in the frequency range.

The damping coefficient k of the curve of $r_a(t)/r_{\max}$ does not depend on time; in contrast, the local value of the damping coefficient of the curve $r(t)/r_{\max}$ decreases with time. Thus, oscillations with a longer oscillation period (initial stage of oscillations) correspond to a larger value of the local damping coefficient; therefore, one can expect the damping $\lambda(\omega)$ at low frequencies to be larger than that at higher frequencies. In fact, if $\Omega < 1$, internal-wave radiation observed is accompanied by great energy losses. If $\Omega > 1$, the energy dissipation is determined by viscous effects (effect of tangential stresses in the boundary layer in the vicinity of the body), as a result of which the energy losses reduce significantly as compared with the case with $\Omega < 1$.

We note that the above interpretation of the behavior of the curve of $r(t)/r_{\max}$ is based on considerations following from the linear theory (in the experiments with $r_{\max}/L < 0.05$). For large initial deflections of the body from the equilibrium, nonlinear effects [15] complicate considerably the entire picture.

Figure 3 and 4 give experimental dependences $C_{11}^{\mu}(\Omega)$ and $C_{11}^{\lambda}(\Omega)$ for a rhombus and a square and curves obtained from relations (11), (12), (15), and (16).

In experiments with a homogeneous fluid, the normalization of $\lambda(\omega)$ and the argument ω by the quantities $\rho_0 NW$ and N from experiments with stratified fluids is of a formal character, and this allows us to compare the experimental results for homogeneous and stratified fluids. In experiments with a homogeneous fluid, the damping coefficient of a rhombus coincide with that of a square, which agrees with the results of [12], allowing for different geometric dimensions used in normalization.

It follows from Figs. 3 and 4 that an abrupt decrease in the added mass coefficient (see Fig. 3) and a local minimum of the damping coefficient (Fig. 4) are observed at an oscillation frequency $\Omega^* \approx 0.7$. At this frequency, the angle between the internal-wave group velocity and the horizontal line $\psi = \arcsin\Omega$ [1] coincides with the slope of the rhombus sides. We note that the behavior of the curves of $C_{11}^{\mu}(\Omega)$ and $C_{11}^{\lambda}(\Omega)$ for the rhombus as $\Omega \to 0.7$

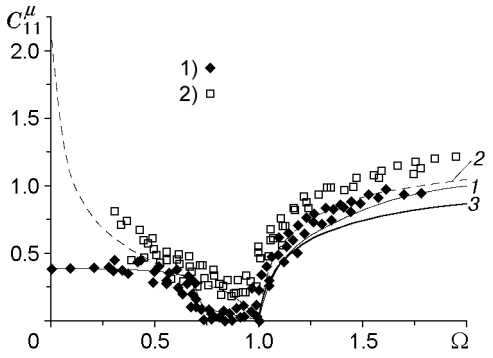

Fig. 3

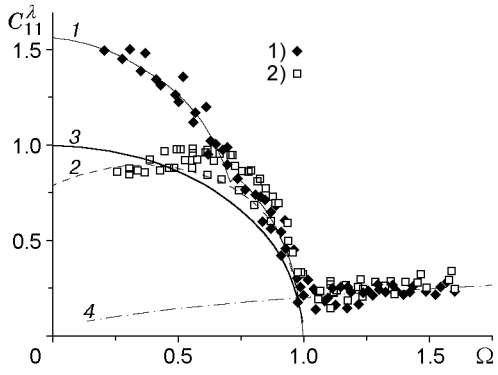

Fig. 4

Fig. 3. Added mass coefficients for horizontal oscillations of a rhombus (1) and a square (2): the curves refer to calculations and points to experiment; curve 3 is a theoretical result of [7] for a circular cylinder.

Fig. 4. Damping coefficients for horizontal oscillations of a rhombus and a square (notation same as in Fig. 3); curve 4 is the approximation of the experimental data for the rhombus and the square in the case of a homogeneous fluid.

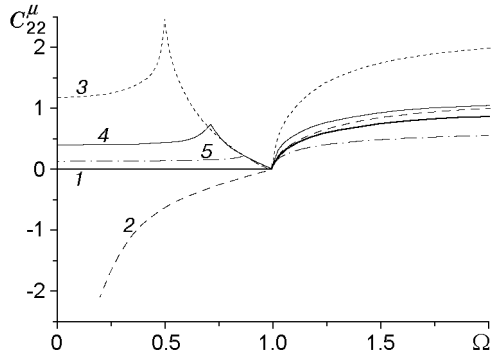

Fig. 5

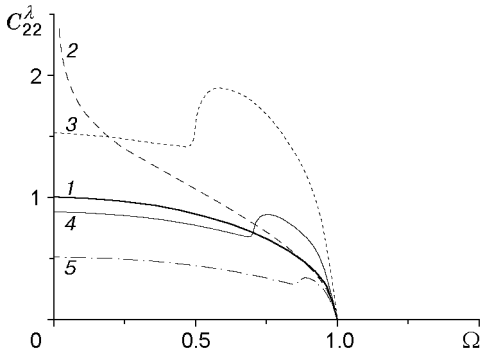

Fig. 6

Fig. 5. Added mass coefficients for vertical oscillations of the rhombus and the square: curve 1 refers to the theoretical data [7] for a circular cylinder, curve 2 to the solution for a square contour, and curves 3–5 refer to the theoretical data for rhombuses with various length ratios of vertical and horizontal diagonals [$1:\sqrt{3}$ for $\chi = 30^\circ$ (3), $1:1$ for $\chi = 45^\circ$ (4), and $\sqrt{3}:1$ for $\chi = 60^\circ$ (5)].

Fig. 6. Damping coefficients for vertical oscillations of the rhombus and the square (notation the same as in Fig. 5).

(limit on the right) is similar to that for the square as $\Omega \to 0$. If $\Omega = 0$, $\psi = 0$, i.e., the internal-wave group velocity is parallel to the upper and lower sides of the square contour.

The experimental results show that viscous effects affect slightly the added mass coefficient (see Fig. 3). The shape of experimental curves of $C_{11}^{\mu}(\Omega)$ is close to the shape of theoretical curves. An insignificant systematic excess of experimental values over theoretical estimates [approximately 5% of the value of $C_{11}^{\mu}(\infty)$] can be explained by the effect of a limited fluid layer thickness in the experimental installation.

If $\Omega > 1$, the damping coefficients $C_{11}^{\lambda}(\Omega)$ for the rhombus and the square in homogeneous and stratified fluids virtually coincide within the experimental error (see Fig. 4). The total damping coefficient $C_{11}^{\lambda}(\Omega)$ can be written as the sum of the wave $C_{11}^{\lambda w}(\Omega)$ and viscous $C_{11}^{\lambda v}(\Omega)$ damping coefficients. If $\Omega < 1$, the damping coefficient for a stratified fluid exceeds considerably that for a homogeneous fluid due to energy expenditure for the internal-wave radiation. As a first rough approximation, $C_{11}^{\lambda} \approx C_{11}^{\lambda w}$ for $\Omega < 1$ and $C_{11}^{\lambda} \approx C_{11}^{\lambda v}$ for $\Omega > 1$. A possible, more detailed, representation of the wave and viscous components is given in [20].

In the present paper, the dynamic characteristics of vertically oscillating bodies were not studied experimentally. The theoretical data on $C^{\mu}_{22}(\Omega)$ and $C^{\lambda}_{22}(\Omega)$ for squares and rhombuses with various side slopes to the horizontal line χ obtained from (11) and (12) are given in Figs. 5 and 6, respectively. As in the case of horizontal oscillations, at frequency $\Omega^* = \sqrt{2}/2 \approx 0.7$, a rhombus with a $1:1$ ratio of diagonal lengths behaves critically: the curve of $C^{\mu}_{22}(\Omega)$ has a local maximum and the curve of $C^{\lambda}_{22}(\Omega)$ exhibits a distinct local minimum. For other ratios of diagonal lengths, the dependences $C^{\mu}_{mn}(\Omega)$ and $C^{\lambda}_{mn}(\Omega)$ and the quantity Ω^* change according to the affine similitude relations (14). In this case, the general characteristics of these dependences remain unchanged (curves 3–5 in Figs. 5 and 6). From elementary geometrical considerations, the critical effects for rhombuses with $\chi = 30$ and 60° take place for $\Omega^* = 0.5$ and $\sqrt{3}/2$.

As $\Omega \to 0$, the square contour enters a special regime in which the internal-wave group velocity is directed almost similarly to the horizontal sides of the contour. Calculations show that as $\Omega \to 0$, the added mass coefficient of the square $C^{\mu}_{22}(\Omega)$ takes large negative values (see Fig. 5), and the damping coefficient $C^{\lambda}_{22}(\Omega)$ increases abruptly (see Fig. 6). For a square contour, we assume the existence of a special critical regime as $\Omega \to 1$, in which the group velocity is directed similarly to the vertical sides of the square contour. However, because the modulus of the group velocity tends to zero, no specificity related to the contour geometry arises as $\Omega \to 1$. If $\Omega = 1$, then $C^{\lambda w}_{mn} = 0$ and $C^{\mu}_{mn} = 0$ for any contours. A circular cylinder has $C^{\mu}_{11} = C^{\mu}_{22}$ and $C^{\lambda}_{11} = C^{\lambda}_{22}$ in accordance with the solution of [7]. Unlike in this case, for cylinders with rhombic and square cross sections, the quantities $C^{\mu}_{mn}(\omega)$ and $C^{\lambda w}_{mn}(\omega)$ differ for vertical and horizontal oscillations. As $\Omega \to \infty$, in an infinite fluid with $N = \text{const}$, the added mass coefficients for rhombuses and squares coincide: $C^{\mu}_{11}(\infty) = C^{\mu}_{22}(\infty) \approx 1.19$.

Conclusions. Thus, in a stratified fluid with horizontal cylinders of polygonal cross sections, hydrodynamic load coefficients change abruptly at the oscillation frequency Ω^* at which the slope of the internal-wave group velocity coincides with the slope of a cylinder side. In the spatial case, these effects are manifested, for example, for bodies formed by rotation of a rhombus about its vertical diagonal. The slope of the internal-wave group velocity coincides with the slope of the characteristic lines of Eq. (1) if $\alpha^2 < 0$. The structure of Eq. (1) coincides with that of the governing equation of the theory of a thin profile in a compressible gas flow (in this case, the parameter $1/\Omega$ acts as a Mach number). The thin wing theory considers a particular case of large Mach numbers, where characteristic lines "lie" on the body surface. The present paper studied an analog of this problem that arises in the theory of internal waves as $\Omega \to \Omega^*$.

The authors thank Yu. D. Chashechkin for his assistance and helpful discussions.

The work was supported by the Russian Foundation for Fundamental Research (Grant No. 00-01-00812) and the Foundation for Young Scientists (Grant No. 1) and the Foundation of Integration Programs (Grant No. 6) of the Siberian Division of the Russian Academy of Sciences.

REFERENCES

1. D. E. Mowbray and B. S. H. Rarity, "A theoretical and experimental investigation of the phase configuration of internal waves of small amplitude in a density stratified liquid," *J. Fluid Mech.*, **28**, Part 1, 1–16 (1967).
2. D. G. Hurley, "The emission of internal waves by vibrating cylinders," *J. Fluid Mech.*, **36**, Part 4, 657–672 (1969).
3. S. A. Makarov, V. I. Neklyudov, and Yu. D. Chashechkin, "Spatial structure of two-dimensional monochromatic internal-wave beams in an exponentially stratified fluid," *Atmos. Ocean Phys.*, **26**, No. 7, 548–554 (1990).
4. B. R. Sutherland, S. B. Dalziel, G. O. Hughes, and P. F. Linden, "Visualization and measurement of internal waves by "synthetic schlieren, Part 1: Vertically oscillating cylinder," *J. Fluid Mech.*, **390**, 93–126 (1999).
5. V. A. Gorodtsov and É. V. Teodorovich, "Energy characteristics of harmonic internal wave generators," *J. Appl. Mech. Tech. Phys.*, **27**, No. 4, 523–529 (1986).
6. R. Y. S. Lay and C.-M. Lee, "Added mass of a spheroid oscillating in a linearly stratified fluid," *Int. J. Eng. Sci.*, **19**, No. 11, 1411–1420 (1981).
7. D. G. Hurley, "The generation of internal waves by vibrating elliptic cylinders, Part 1: Inviscid solution," *J. Fluid Mech.*, **351**, 105–118 (1997).
8. D. G. Hurley and G. Keady, "The generation of internal waves by vibrating elliptic cylinders, Part 2: Approximate viscous solution," *ibid.*, **351**, 119–139 (1997).
9. E. V. Ermanyuk, "The use of impulse response functions for evaluation of added mass and damping coefficient of a circular cylinder oscillating in linearly stratified fluid," *Exp. Fluids.*, **28**, 152–159 (2000).

10. E. V. Ermanyuk, "The rule of affine similitude for the force coefficients of a body oscillating in uniformly stratified fluid," *Exp. Fluids.*, **32**, 242–251 (2002).
11. S. B. Dalziel, "Synthetic schlieren measurements of internal waves generated by oscillating a square cylinder," in: *Proc. 5th Intern. Symp. on Stratified Flows* (Vancouver, Canada, July 10–13, 2000), Vol. 2, Univ. of British Columbia, Vancouver (2000), pp. 743–748.
12. P. W. Bearman, V. G. Downie, J. M. R. Graham, and E. D. Obasaju, "Forces on cylinders in viscous oscillatory flow at low Keulegan–Carpenter numbers," *J. Fluid Mech.*, **154**, 337–356 (1985).
13. Yu. V. Kistovich and Yu. D. Chashechkin, "Generation of monochromatic internal waves in a viscous fluid," *J. Appl. Mech. Tech. Phys.*, **40**, No. 6, 1020–1028 (1999).
14. Yu. S. Il'inykh, S. A. Smirnov, and Yu. D. Chashechkin, "Generation of harmonic internal waves in a viscous stratified fluid," *Izv. Ross. Akad. Nauk, Mekh. Zhidk. Gaza*, No. 6, 141–148 (1999).
15. V. V. Levitskii and Yu. D. Chashechkin, "Natural oscillations of a neutrally buoyant body in a continuously stratified fluid," *Izv. Ross. Akad. Nauk, Mekh. Zhidk. Gaza*, No. 5, 39–52 (1999).
16. V. A. Gorodtsov and É. V. Teodorovich, "On the generation of internal waves in the presence of uniform straight-line motion of local and non-local sources," *Atmos. Ocean. Phys.*, **16**, No. 9, 699–704 (1980).
17. J. N. Newman, *Marine Hydrodynamics*, MIT Press, Cambridge (1977).
18. A. I. Korotkin, *Reference Book on Added Masses of a Ship* [in Russian], Sudostroenie, Leningrad (1986).
19. V. A. Vladimirov and K. I. Il'in, "Slow motions of a solid in a continuously stratified fluid," *J. Appl. Mech. Tech. Phys.*, **32**, No. 2, 194–199 (1991).
20. E. V. Ermanyuk and N. V. Gavrilov, "Force on a body in a continuously stratified fluid, Part 1: Circular cylinder," *J. Fluid Mech.*, **451**, 421–443 (2002).
21. M. D. Huskind, "Methods of hydrodynamics in problems of navigability of ships on waves," *Tr. TsAGI*, No. 603, 1–74 (1947).